Electronic structure and molecular orientation of pentacene thin films on ferromagnetic $La_{0.7}Sr_{0.3}MnO_3$

Fenghong Li,[1,*] Patrizio Graziosi,[2] Qun Tang,[1] Yiqiang Zhan,[1] Xianjie Liu,[1] Valentin Dediu,[2] and Mats Fahlman[1,†]
[1]*Department of Physics, Chemistry and Biology, Linköping University, 581 83 Linköping, Sweden*
[2]*Istituto per lo Studio di Materiali Nanostrutturati–Consiglio Nazionale delle Ricerche (ISMN-CNR), via Gobetti 101, 40129 Bologna, Italy*

(Received 15 October 2009; revised manuscript received 9 April 2010; published 11 May 2010)

Pentacene thin films deposited on a ferromagnetic electrode, $La_{0.7}Sr_{0.3}MnO_3$ (LSMO), have been studied using near-edge x-ray absorption fine structure (NEXAFS), ultraviolet photoemission spectroscopy (UPS), and atomic force microscopy (AFM). Here we present electronic structure and molecular orientation of pentacene thin film on LSMO. No evidence related to covalent bonding or significant charge transfer between pentacene and LSMO has been found in the NEXAFS or UPS results. UPS measurements suggest that the vertical ionization potential of pentacene on LSMO is 4.9 eV. Our results extracted from NEXAFS indicate that molecular long axis of pentacene stands on the LSMO substrate surface with a tilt angle of about $22° \pm 2°$ between the main molecular axis and the substrate surface normal. AFM images show the terracelike crystalline grain formed by stacking pentacene crystalline layers and a rough crystal-layer spacing of 14–15 Å. Findings deduced from UPS, NEXAFS, and AFM consistently demonstrate that pentacene stands on LSMO with a tilt angle.

DOI: 10.1103/PhysRevB.81.205415 PACS number(s): 81.07.Pr, 79.60.Fr, 85.75.−d, 78.70.Dm

I. INTRODUCTION

The 2007 Nobel Prize in physics was awarded to Albert Fert and Peter Grünberg for the discovery of giant magnetoresistance (GMR) which is considered as the birth of spintronics.[1,2] Spintronics, an extension to electronics, describes technology that makes use of the spin state of electrons. The most successful spintronic device to date is the spin valve, due to their widespread application in disk read/write heads. This device utilizes a layered structure of thin films of magnetic materials which changes electrical resistance depending on the applied magnetic field direction. Organic spintronics is a new branch of the field of molecular electronics.[3] It deals with the injection and detection of spin-polarized carriers in organic semiconductors by means of spin-valve devices. Injection and detection of spins is realized by a pair of ferromagnetic electrodes, for example, LSMO (Ref. 4) and cobalt (Co) (Ref. 5) whereas the transport and manipulation of spins is realized in the organic semiconductors between the two ferromagnets. In order to understand spin injection and detection in spin-valve devices, it is critical to study the organic-ferromagnetic interfaces. Organic molecular materials offer a new and highly promising route toward spintronics mainly due to the advantage of weak spin-orbit coupling in organic molecules,[6] enabling the preservation of spin coherence over times and distances much longer than in conventional, inorganic semiconductors. Concerning spin injection, half metals such as LSMO are especially attractive since the conductivity mismatch limitation for direct spin-polarized injection at the ferromagnetic-semiconductor interface does not apply to these fully spin-polarized systems. Prototype spin valves based on LSMO and organic semiconductors have recently been demonstrated.[3,5] In particular planar-type spin valves based on a pentacene thin film with LSMO electrodes have been achieved, in which it was found that the spins were scattered by grain boundaries, carriers, and impurities in films.[7] Therefore, it is necessary to characterize the nanoscale structure to establish relationships between chemical structure, processing, morphology, fundamental electronic properties, and performance. Morphology, energy-level alignment, molecule-molecule or molecule-substrate interaction, and molecular orientation of pentacene thin films on various nonferromagnetic substrates including inorganic and organic materials have been investigated extensively.[8–14] However so far a systematical study of pentacene on ferromagnetic substrates has not reported yet. Here we focus on electronic structure at the interface/surface and molecular orientation of pentacene thin films on LSMO surface, which largely determine spin injection, using ultraviolet photoelectron spectroscopy (UPS), near-edge x-ray absorption fine structure (NEXAFS), and atom force microscopy (AFM).

II. EXPERIMENTAL

The LSMO films were deposited by pulsed electron-deposition technique (channel spark ablation) following the protocols reported previously.[15] Pentacene was used as delivered from Sigma-Aldrich. Organic thin films were deposited on LSMO substrates by thermal evaporation *in situ* from a Knudsen cell in vacuum with a base pressure 10^{-8} mbar. When the LSMO substrates are annealed in ultrahigh vacuum and then in oxygen atmosphere for half an hour at ~500 °C, the work function (WF) of such a clean LSMO is 4.8–4.9 eV.[16] However, this treatment procedure is not applicable for the practical device fabrication. For many applications, the electrode surfaces are only cleaned by *ex site* procedures using ultrasonic treatment in organic solvents prior to the deposition of organic materials.[5] 4.0–4.2 eV is the WF of LSMO exposed to ambient atmosphere and ultrasonically cleaned in acetone and isopropanol prior to putting into the vacuum chamber for the measurement of UPS because of the contaminants on surface.[17,18] In order to remove

organic contaminants and increase oxygen stoichiometry on LSMO surface, we used a different *ex situ* cleaning procedure, i.e., after ultrasonic treatment in organic solvents, LSMO is heated in the solution so-called TL1 (Ref. 19) ($5H_2O$, $1NH_4OH$, and $1H_2O_2$) at 85 °C for 5–10 min. The WF of LSMO treated by TL1 is 4.6–4.9 eV depending on treatment time.

The UPS characterizations were carried out with monochromatized HeI radiation at 21.2 eV for every step of organic molecular deposition. The deposition process was additionally aided by x-ray photoelectron spectroscopy that was used to monitor the thickness of organic-material overlayer from the attenuation of the substrate core-level signal. Polarized x-ray absorption spectroscopy (XAS) measurements were performed at beam line D1011 of the MAX-II storage ring, located at the MAX Laboratory for Synchrotron Radiation Research in Lund, Sweden. X-ray absorption spectra of Mn *L* edge were recorded with the electron-emission direction along the sample normal, for which the incident angle of the beam was 50°. NEXAFS spectra of C *K* edge were collected in the total electron yield (TEY) mode by measuring the sample current at the five incident angles of the beam which were 10°, 30°, 50°, 70°, and 90°, respectively. Both the photon linewidth and the energy resolution of the electron analyzer were kept well below 100 meV. The raw data have been corrected for the energy dependence of the incident x-ray beam and subsequently normalized to have the same absorption edge step well-above threshold. The surface morphology of pentacene thin films was imaged by a Dimension 3100 AFM. AFM measurements were performed under ambient conditions using a Digital Instrument Multimode Nanoscope IIIA operating in the tapping mode. The thickness value of 20 nm pentacene in the AFM images was obtained directly from AFM measurements while the thickness value of a (sub)monolayer about 1 nm was estimated by evaporation rate and time. The thickness values mentioned in the NEXAFS and UPS spectroscopic measurements were estimated by the attenuation of La 4*d* core-level signal of LSMO substrates. It should be noted that this procedure to determine the film thickness is only correct for a layer-by-layer growth of the organic film. If the organic film is not uniform, this method underestimates the film thickness. We estimate the error of film-thickness determination to be on the order of 20%.

III. RESULTS AND DISCUSSION

The electrical and magnetic properties of manganites are mainly determined by the Mn valence, which is traditionally described as a mixture of Mn^{3+} and Mn^{4+}. Recently by means of XAS, de Jong *et al.*[20,21] and Valencia *et al.*[22,23] have presented evidence of the presence of Mn^{2+} ions on LSMO and $La_{2/3}Ca_{1/3}MnO_3$ (LCMO) thin films, respectively. Moreover the formation of divalent Mn can be a general feature occurring on lanthanum-manganese perovskites, particularly when exposed to ambient atmosphere.[22] Even though de Jong *et al.*[21] concluded that the presence of undesirable Mn^{2+} at the surface would not form a major obstacle for spin injection, Valencia *et al.*[22] have found that LCMO

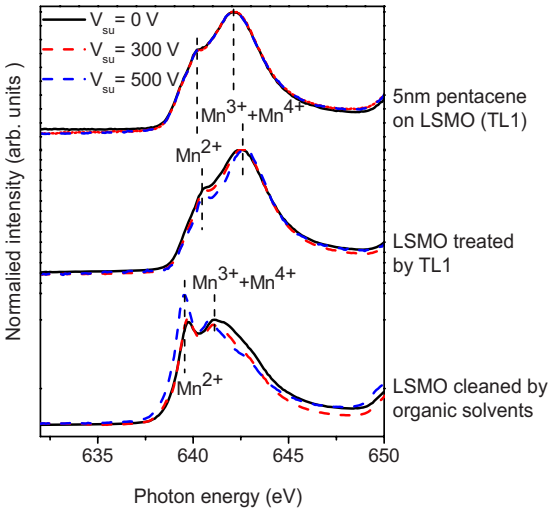

FIG. 1. (Color online) X-ray absorption spectra of Mn *L* edge of LSMO exposed to ambient atmosphere for three weeks and ultrasonically cleaned in acetone and isopropanol (bottom), LSMO treated by TL1 (middle), and 5 nm pentacene vacuum deposited on LSMO treated by TL1 (top). All spectra were collected by means of both total yield mode (black line) and partial yield mode (300 V suppression, red dashed line and 500 V suppression, blue dashed line, which has a strongest intensity at 639.7 eV in the bottom spectra and a weakest intensity at 640.6 eV in the middle spectra).

samples exposed to ambient atmosphere for weeks exhibited reduced magnetic and magnetotransport properties due to the appearance of Mn^{2+} in addition to the expected Mn^{3+} and Mn^{4+}. Therefore, it is necessary to decrease Mn^{2+} ions at the surface as greatly as possible. In this study, we use TL1 to treat LSMO as described in experimental section. After TL1 treatment, not only WF of LSMO increased from 4.3 to 4.7 eV but also the peak corresponding to Mn^{2+} became weakened due to the removal of some contaminants and an increase in oxygen content at the surface. Figure 1 shows Mn *L*-edge XAS spectra in the region of the L_3 transition, namely, $2p_{3/2}$ hole state, for LSMO exposed to ambient atmosphere for three weeks and cleaned by organic solvent prior to measurement, LSMO treated by TL1 prior to measurement and 5 nm pentacene *in situ* vacuum deposited on LSMO treated TL1. The spectra of all samples were obtained using TEY mode (without suppression, black line) and partial electron yield (PEY) mode (300 V suppression, red dashed line; 500 V suppression, blue dashed line) resulting in probing different depths. It is clear that there exist abundant Mn^{2+} ions corresponding to the peak at 639.7 eV in addition to the mixture of Mn^{3+} and Mn^{4+} ions corresponding to the peak at 641.1 eV for LSMO substrate exposed to ambient atmosphere for three weeks (bottom spectra). PEY mode is more sensitive to surface than TEY. Particularly PEY mode applying 500 V suppression probes an about 1-nm-thin surface region. As expected, a sharp peak at 639.7 eV produced by Mn^{2+} ions become stronger and stronger when secondary electron suppression voltage V_{su} changes from 0 and 300 to 500 V. It indicates that there are more Mn^{2+} ions at the surface than in the bulk. However after TL1 treatment, the sharp peak at 639.7 eV disappears as shown in the middle spectra of Fig. 1. There is a main peak at 642.5 eV accompanied by

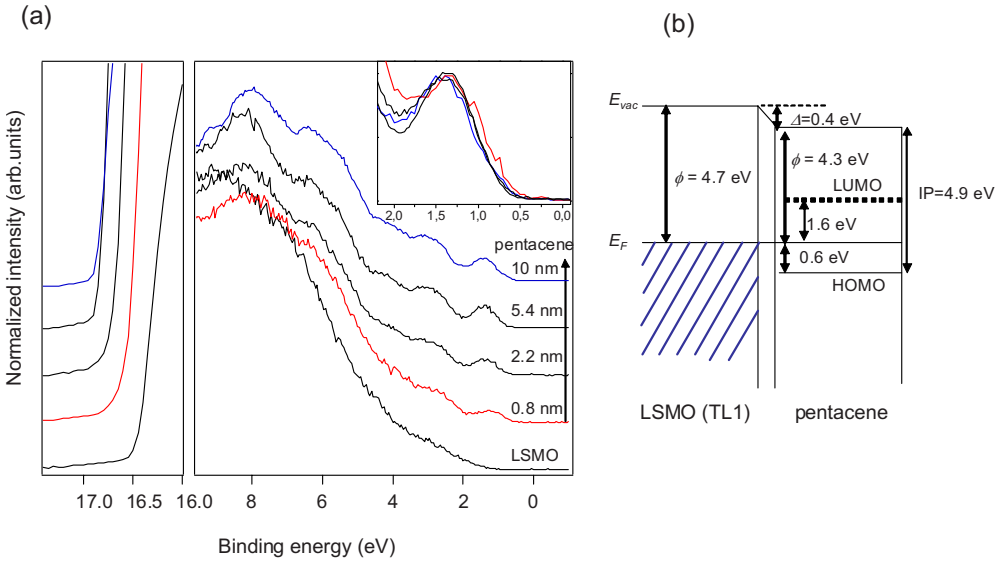

FIG. 2. (Color online) (a) UPS spectra of LSMO treated by TL1 and pentacene thin films with thickness from 0.8 nm (red line) to 10 nm (blue line) on LSMO. Inset shows valence-band spectra blown up from −0.5 to 2.5 eV. (b) Energy-level alignment diagram derived from (a) for a bulk pentacene thin film on LSMO treated by TL1.

a shoulder at 640.6 eV. More importantly the intensity of this shoulder peak becomes weak gradually with increasing suppression voltages from 0 and 300 to 500 V. It means that TL1 treatment results in a removal of Mn^{2+} due to an increase in oxygen content at the surface of LSMO. In order to check the influence of the deposition of pentacene on the oxidized states of Mn at the surface of LSMO, XAS spectra of 5 nm pentacene on LSMO treated by TL1 were also collected using V_{su}=0, 300, and 500 V. A main peak at 642.1 eV with a shoulder around 640.2 eV appears in the top spectra. An obvious difference cannot be found for the three probing depths. The reason may be an island growth of pentacene on LSMO which will be discussed in the following AFM images. The shape and peak position of the top spectra for after the deposition of pentacene do not show an obvious difference from the middle spectra for before the deposition of pentacene. This suggests an absence of covalent bonding and no significant charge transfer at the interface.

Orientation-dependent vertical ionization potentials (IP) of ordered organic semiconductor thin films have been investigated recently.[11,12,24–26] The IP of pentacene depends dramatically on molecular orientation on various substrates.[11,12,26] Electronic structure and energy-level alignment at the interface between LSMO and pentacene with the evolution of thickness were investigated using UPS. Figure 2(a) shows the UPS spectra of LSMO treated by TL1, pentacene submonolayer (0.8 nm) and three pentacene multilayer (2.2, 5.4, and 10 nm) samples deposited *in situ* on LSMO at room temperature in the secondary electron cut-off region and the valence-band region. Here we simply refer to more or less 1 nm pentacene as a submonolayer since at this range of thickness the pentacene film is not able to fully cover the LSMO. The WF is defined by the secondary electron cutoff in the left-hand panel. When a pentacene submonolayer is vapor deposited on the LSMO substrate, WF of the LSMO substrate slightly changes from 4.7 to 4.6 eV. With increasing pentacene deposition, the WF of pentacene thin films on LSMO substrates eventually reaches a steady value 4.3 eV at full coverage of the LSMO surface indicating an interface dipole energy of 0.4 eV for the pentacene/LSMO contact. The resulting WF is similar to that of "dirty" LSMO (Ref. 18) and the interface dipole is thus likely due to the so-called push-back effect.[27] From the experimental UPS spectra depicted in Fig. 2(a), the vertical IP of pentacene vs vacuum level can be determined from the onset of highest occupied molecular orbital (HOMO) in the valence-band spectra and WF. In the valence-band spectra, the features of pentacene become gradually visible with increasing the coverage of pentacene on LSMO. The onset of HOMO for 0.8 nm pentacene is around 0.5 eV. IP of the submonolayer pentacene is estimated to be 5.1 eV because its WF is 4.6 eV. The 2.2 nm pentacene thin film also has the IP of 5.1 eV due to the onset of HOMO of 0.6 eV and WF of 4.5 eV. The IP value equal to 5.1 eV is in agreement with one of unordered pentancene thin film on highly ordered pyrolytic graphite (HOPG) (Ref. 11). It is possible that the first few monolayers of pentacene aggregate randomly on LSMO. However when thickness of pentacene reaches 5.4 nm, the IP changes to 4.9 eV because the onset of HOMO is still 0.6 eV while WF is decreased to 4.3 eV. Further increasing the coverage of pentacene up to 10 nm does not lead to a further change in IP because onset of HOMO and WF reach steady value 0.6 eV and 4.3 eV, respectively. The IP value equal to 4.9 eV is same with value reported by Duhm *et al.*[28] for pentacene on SiO_2 in standing orientation. Figure 2(b) shows energy-level alignment derived from left hand in Fig. 2(a) for a bulk pentacene thin film on LSMO substrate treated by TL1. The IP and onset of HOMO versus Fermi level have been measured. The position of the pentacene lowest unoccupied molecular orbital (LUMO) level was estimated by the transport gap of 2.2 eV (Refs. 13 and 28) instead of the optical gap.

No significant modification of the spectral features in the region between HOMO level and Fermi level is observed as shown in inset of Fig. 2(a). Covalent bonding and/or substan-

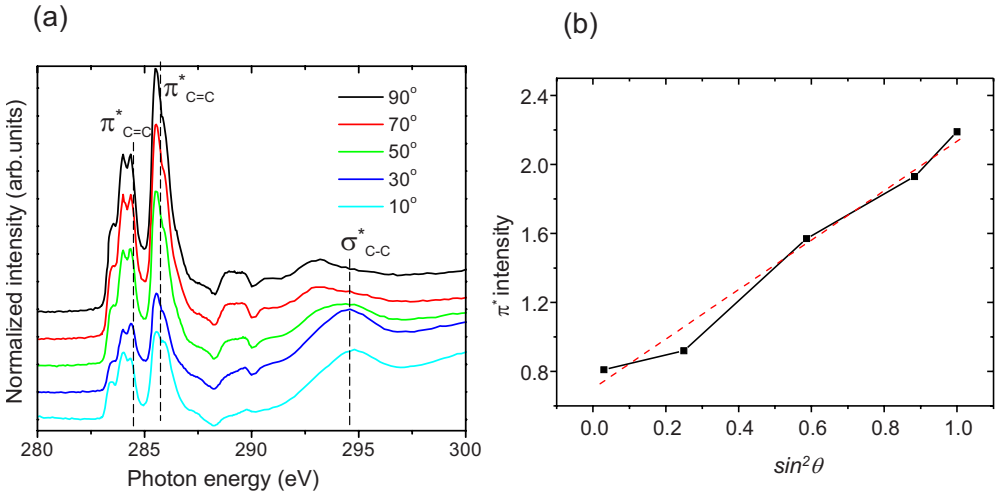

FIG. 3. (Color online) (a) C *K*-edge NEXAFS spectra collected at different angles (90°, black line; 70°, red line; 50°, green line; 30°, blue line; and 10°, cyan line) of the beam relative to the substrate plane for a 5 nm pentacene thin film deposited on LSMO treated by TL1. (b) π^* intensity normalized versus the squared sine of incident angle.

tial charge transfer at the interface can thus be ruled out, supporting the assignation of the interface dipole origin to the push-back effect. This is in agreement with the results from Mn *L*-edge XAS spectra in Fig. 1.

The carbon *K*-edge NEXAFS spectra were collected with linearly polarized synchrotron radiation at several incident angles relative to substrate plane, as shown in Fig. 3(a) to characterize the molecular orientation of pentacene on LSMO. The remarkable variations in intensity of peaks corresponding to π^* and σ^* resonances as a function of polarization angles clearly indicate the formation of ordered pentacene layers with a preferential direction of orientation.[8] The most prominent absorbance is the carbon-carbon $1s \rightarrow \pi^*$ transition, which is split here into several peaks in the area from 282.5 to 287.5 eV, in which absorption features lower than 285 eV correspond to empty LUMO π^* state while absorption features higher than 285 eV correspond to empty LUMO+1 π^* state.[8] The resonance close to 295 eV is carbon-carbon $1s \rightarrow \sigma^*$ transition of the single bond. Both transitions exhibit angular variation. The π^* orbital intensity is greatest near normal incidence and σ^* orbital intensity is greatest near grazing incidence. The orientation of pentacene can be extracted from Fig. 3(a) by considering the pentacene carbon-carbon molecular-orbital orientation. π^* intensity versus the square sine of incident angle is roughly plotted in Fig. 3(b). According to the following equations,[29,30] the conjugated plane normal has an average orientation angle of about $68° \pm 2°$ away from surface normal:

$$I = \frac{A}{3}(1 + K) - \frac{AK}{2}\sin^2\theta,$$

$$K = 3\cos^2\alpha - 1.$$

Here, A is a constant, roughly analogous to the extinction coefficient of conventional optical spectroscopy, θ is the angle of the beam relative to the substrate plane, and α is the angle of the vector orbital relative to substrate normal. We here assume that the polarization factor is 1 at the D1011 end station.

Based on such analysis, the molecular long axis of pentacene is found to stand on the LSMO substrate surface with a tilt angle of about $22° \pm 2°$ between the main molecular axis and the substrate surface normal. It is quite similar to the molecular orientation of thermally evaporated pentacene thin film on self-assembled monolayer (SAM) (Ref. 8) and inert substrates.[30,31]

AFM images of pentacene thin films on LSMO give NEXAFS results a cogent support by images as well as a layer height value. Figure 4 demonstrates AFM images of (a) bare LSMO, (b) 1 nm pentacene, and (c) 20 nm pentacene thin films. First the morphology of the first submonolayer pentacene on LSMO was studied using AFM compared to bare LSMO. Figure 4(b) shows AFM images of 1 nm pentacene on LSMO that resemble the morphology of the first monolayers pentacene on inert substrates such as silicon oxide[32] or passivated Si.[33] When deposited on LSMO, pentacene molecules diffuse on the substrate nucleating monolayer islands with fractal shapes. Conventional concepts of diffusion-mediated growth apply to the formation of the first pentacene layer on the inert substrates.[34,35] Diffusion-mediated growth involves four qualitatively different steps.[36] Initially, molecules diffuse on an almost bare substrate and a stable nucleus is formed when a critical number of them meet. In a second (intermediate) step, adsorbates still nucleate new islands but also start aggregating into existing ones. Later, in the aggregation regime, the incoming material aggregates into the existing islands only. Finally, islands coalesce. Interestingly each of four steps can be observed clearly in Fig. 4(b). Insets from local enlargement in Fig. 4(b1) correspond to first step. Top inset corresponds to the condition before nucleation while a preisland with terrace is nucleating as shown in bottom inset. More importantly step height of the terrace equal to 1.4–1.5 nm is obtained from the bottom inset. Some islands corresponding to second or third step exist in the green circle while the red circle highlights a happened coalescence in the Fig. 4(b2).

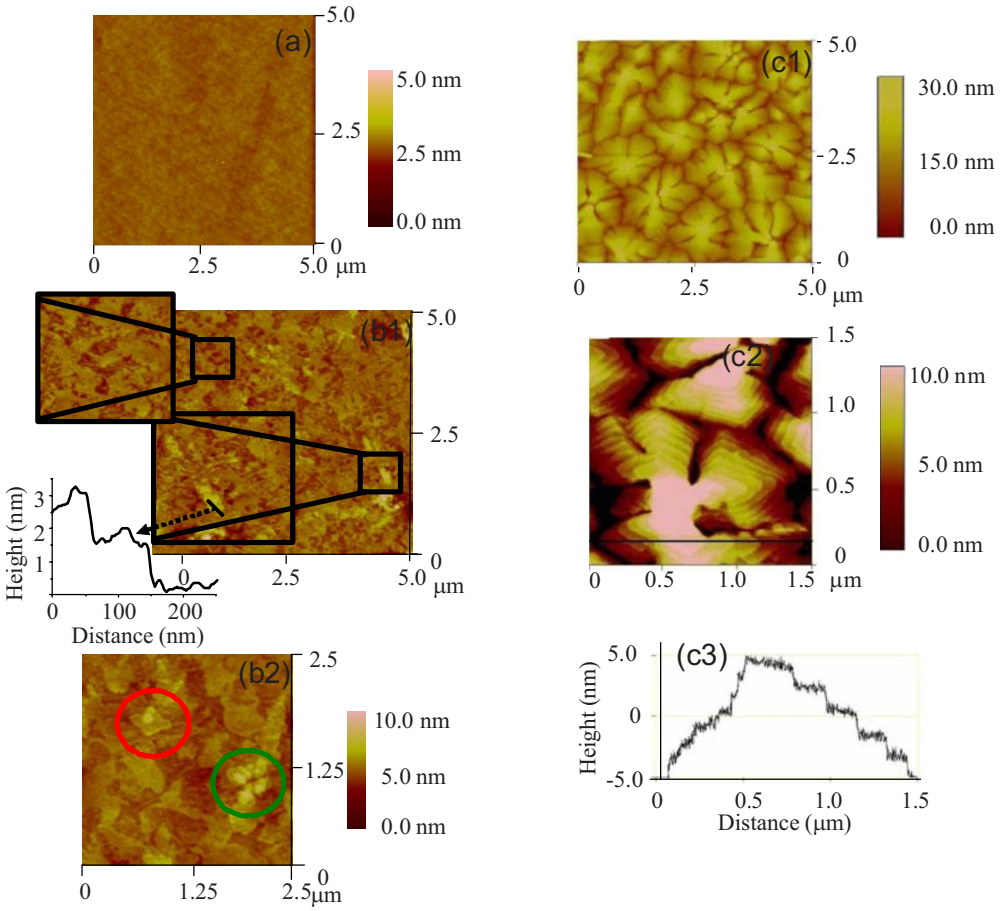

FIG. 4. (Color online) AFM images of (a) bare LSMO, (b) 1 nm pentacene, and (C) 20 nm pentacene thin films on LSMO. (b) shows different steps for diffusion-mediated growth of a submonolayer (1nm) of pentacene on the LSMO substrate and step height of the terrace equal to 1.4–1.5 nm obtained from the bottom inset of (b1). (c) shows AFM images of a 20 nm pentancene thin film deposited on LSMO with the sizes of 5×5 μm^2 (c1) and local enlargement by the area of 1.5×1.5 μm^2 (c2) which displays an obvious stepwise structure in each grain and where height line gives a rough step height of stacking pentacene crystalline layers (c3).

Second the morphology of bulk pentacene thin films on LSMO was characterized using AFM as well. As shown in Fig. 4(c) for images of 20 nm pentacene vapor deposited on LSMO, the terracelike crystalline grains are formed by stacking pentacene crystalline layers. The average grain size of pentacene on LSMO is 1.0–1.5 μm and each grain has a layered structure in Fig. 4(c1). A rough crystal layer spacing of 14–15 Å can be derived from Figs. 4(c2) and 4(c3), which is very similar to the step height of 1.5 nm for 10 nm terracelike pentacene on ITO substrate[37] and almost same to the value from Fig. 4(b1). This value is close to the molecular long axis edge on height [16.5 Å (Ref. 38)], which also implies that the pentacene molecules in this structure are oriented in standing mode on LSMO substrate with a somewhat tilted angle related to the substrate surface normal.

It has been reported that there is a facile charge transport within each two-dimensional herringbone-packed pentacene crystal layer but negligible charge transport through the vertically stacked layer direction. As a result, the pentacene films on LSMO potentially exhibits a high hopping resistance in the vertical direction, which is nearly parallel to the substrate-standing molecules. The interfaces are crucial for both injection (GMR) and tunnelling (tunnel magnetoresistance) devices. While injection and transport could be accompanied by quite high resistance in that the pentacene molecules stand up on the injector LSMO surface, this configuration could be extremely appealing for tunnelling spintronic devices. It should be noted that in other cases pentacene molecules may lay down on the injector surface and allow good injection efficiency.

IV. CONCLUSION

No evidence related to covalent bonding or significant charge transfer between pentacene and LSMO has been found in the XAS of Mn *L* edge or UPS results. In addition, an interface dipole of 0.4 eV reduces the work function to 4.3 eV upon pentacene film deposition, mainly due to the push-back effect. UPS measurements suggest that the vertical IP of pentacene on LSMO is 4.9 eV, same as the value reported for pentacene on SiO_2 in standing orientation. Findings deduced from NEXAFS, AFM, and UPS spectra consistently demonstrate that pentacene stands on LSMO with a tilt angle. The results extracted from NEXAFS demonstrate that

molecular long axis of pentacene stands on the LSMO substrate surface with a tilt angle of about $22° \pm 2°$ between the main molecular axis and the substrate surface normal. AFM images further give an additional support that the terracelike crystalline grain is formed by stacking pentacene crystalline layers and pentacene molecules in this structure are tilted in standing mode on LSMO substrate.

ACKNOWLEDGMENTS

This work was carried out within the EU Integrated Project OFSPIN (EU-FP6-STREP). In general, the Surface Physics and Chemistry division is supported by the Swedish Research Council (project grant and Linneus center) and the Knut and Alice Wallenberg Foundation.

*Present address: State Key Laboratory for Supramolecular Structure and Materials, Jilin University, Changchun 130012, China; fhli@jlu.edu.cn

†mats.fahlman@itn.liu.se

[1] G. Binasch, P. Grünberg, F. Saurenbach, and W. Zinn, Phys. Rev. B **39**, 4828 (1989).

[2] M. N. Baibich, J. M. Broto, A. Fert, F. Nguyen Van Dau, F. Petroff, P. Etienne, G. Creuzet, A. Friederich, and J. Chazelas, Phys. Rev. Lett. **61**, 2472 (1988).

[3] V. A. Dediu, L. E. Hueso, I. Bergenti, and C. Taliani, Nature Mater. **8**, 707 (2009).

[4] V. Dediu, M. Murgia, F. C. Matacotta, C. Taliani, and S. Barbanera, Solid State Commun. **122**, 181 (2002).

[5] Z. H. Xiong, D. Wu, Z. V. Vardeny, and J. Shi, Nature (London) **427**, 821 (2004).

[6] P. A. Bobbert, W. Wagemans, F. W. A. van Oost, B. Koopmans, and M. Wohlgenannt, Phys. Rev. Lett. **102**, 156604 (2009).

[7] T. Ikegami, I. Kawayama, M. Tonouchi, S. Nakao, Y. Yamashita, and H. Tada, Appl. Phys. Lett. **92**, 153304 (2008).

[8] M. Chiodi, L. Gavioli, M. Beccari, V. Di Castro, A. Cossaro, L. Floreano, A. Morgante, A. Kanjilal, C. Mariani, and M. G. Betti, Phys. Rev. B **77**, 115321 (2008).

[9] W. S. Hu, Y. T. Tao, Y. J. Hsu, D. H. Wei, and Y. S. Wu, Langmuir **21**, 2260 (2005).

[10] Y. Zheng, D. C. Qi, N. Chandrasekhar, X. Y. Gao, C. Troadec, and A. T. S. Wee, Langmuir **23**, 8336 (2007).

[11] H. Fukagawa, H. Yamane, T. Kataoka, S. Kera, M. Nakamura, K. Kudo, and N. Ueno, Phys. Rev. B **73**, 245310 (2006).

[12] I. Salzmann, S. Duhm, G. Heimel, M. Oehzelt, R. Kniprath, R. L. Johnson, J. P. Rabe, and N. Koch, J. Am. Chem. Soc. **130**, 12870 (2008).

[13] N. Koch, J. Ghijsen, R. L. Johnson, J. Schwartz, J. J. Pireaux, and A. Kahn, J. Phys. Chem. B **106**, 4192 (2002).

[14] N. Koch, A. Kahn, J. Ghijsen, J. J. Pireaux, J. Schwartz, R. L. Johnson, and A. Elschner, Appl. Phys. Lett. **82**, 70 (2003).

[15] V. Dediu, L. E. Hueso, I. Bergenti, A. Riminucci, F. Borgatti, P. Graziosi, C. Newby, F. Casoli, M. P. De Jong, C. Taliani, and Y. Zhan, Phys. Rev. B **78**, 115203 (2008).

[16] Y. Q. Zhan, I. Bergenti, L. E. Hueso, V. Dediu, M. P. de Jong, and Z. S. Li, Phys. Rev. B **76**, 045406 (2007).

[17] M. P. de Jong, V. A. Dediu, C. Taliani, and W. R. Salaneck, J. Appl. Phys. **94**, 7292 (2003).

[18] M. Grobosch, K. Dorr, R. B. Gangineni, and M. Knupfer, Appl. Phys. Lett. **92**, 023302 (2008).

[19] A. Andersson, N. Johansson, P. Bröms, N. Yu, D. Lupo, and W. R. Salaneck, Adv. Mater. **10**, 859 (1998).

[20] M. P. de Jong, I. Bergenti, V. A. Dediu, M. Fahlman, M. Marsi, and C. Taliani, Phys. Rev. B **71**, 014434 (2005).

[21] M. P. de Jong, I. Bergenti, W. Osikowicz, R. Friedlein, V. A. Dediu, C. Taliani, and W. R. Salaneck, Phys. Rev. B **73**, 052403 (2006).

[22] S. Valencia, A. Gaupp, W. Gudat, L. Abad, L. Balcells, A. Cavallaro, B. Martinez, and F. J. Palomares, Phys. Rev. B **73**, 104402 (2006).

[23] S. Valencia, A. Gaupp, W. Gudat, L. Abad, L. Balcells, and B. Martinez, Phys. Rev. B **75**, 184431 (2007).

[24] S. Duhm, G. Heimel, I. Salzmann, H. Glowatzki, R. L. Johnson, A. Vollmer, J. P. Rabe, and N. Koch, Nature Mater. **7**, 326 (2008).

[25] W. Chen, H. Huang, S. Chen, Y. L. Huang, X. Y. Gao, and A. T. S. Wee, Chem. Mater. **20**, 7017 (2008).

[26] N. Koch, I. Salzmann, R. L. Johnson, J. Pflaum, R. Friedlein, and J. P. Rabe, Org. Electron. **7**, 537 (2006).

[27] X. Crispin, V. Geskin, A. Crispin, J. Cornil, R. Lazzaroni, W. R. Salaneck, and J. L. Bredas, J. Am. Chem. Soc. **124**, 8131 (2002).

[28] S. Duhm, I. Salzmann, G. Heimel, M. Oehzelt, A. Haase, R. L. Johnson, J. P. Rabe, and N. Koch, Appl. Phys. Lett. **94**, 033304 (2009).

[29] J. Stöhr, *NEXAFS Spectroscopy* (Springer, New York, 1992).

[30] Z. Bao and J. J. Locklin, *Organic Field-Effect Transistors* (CRC Press, Boca Raton, 2007).

[31] F. Zheng, B. N. Park, S. Seo, P. G. Evans, and F. J. Himpsel, J. Chem. Phys. **126**, 154702 (2007).

[32] R. Ruiz, B. Nickel, N. Koch, L. C. Feldman, R. F. Haglund, A. Kahn, and G. Scoles, Phys. Rev. B **67**, 125406 (2003).

[33] F.-J. Meyer zu Heringdorf, M. C. Reuter, and R. M. Tromp, Nature (London) **412**, 517 (2001).

[34] R. Ruiz, D. Choudhary, B. Nickel, T. Toccoli, K. C. Chang, A. C. Mayer, P. Clancy, J. M. Blakely, R. L. Headrick, S. Iannotta, and G. G. Malliaras, Chem. Mater. **16**, 4497 (2004).

[35] R. Ruiz, B. Nickel, N. Koch, L. C. Feldman, R. F. Haglund, Jr., A. Kahn, F. Family, and G. Scoles, Phys. Rev. Lett. **91**, 136102 (2003).

[36] J. G. Amar, F. Family, and P. M. Lam, Phys. Rev. B **50**, 8781 (1994).

[37] R. Naito, S. Toyoshinia, T. Ohashi, T. Sakurai, and K. Akimoto, Jpn. J. Appl. Phys., Part 1 **47**, 1416 (2008).

[38] G. Yoshikawa, T. Miyadera, R. Onoki, K. Ueno, I. Nakai, S. Entani, S. Ikeda, D. Guo, M. Kiguchi, H. Kondoh, T. Ohta, and K. Saiki, Surf. Sci. **600**, 2518 (2006).